Title
Disulfide Linkage and Structure of Highly Stable Yeast-derived Virus-like Particles of Murine Polyomavirus*

Journal
Journal of Biological Chemistry, 289(15)

ISSN
0021-9258

Authors
Simon, Claudia
Klose, Thomas
Herbst, Sabine
et al.

Publication Date
2014-04-01

DOI
10.1074/jbc.m113.484162

Peer reviewed

THE JOURNAL OF BIOLOGICAL CHEMISTRY VOL. 289, NO. 15, pp. 10411–10418, April 11, 2014
Published in the U.S.A.

Disulfide Linkage and Structure of Highly Stable Yeast-derived Virus-like Particles of Murine Polyomavirus*[S]

Received for publication, September 25, 2013, and in revised form, February 22, 2014 Published, JBC Papers in Press, February 24, 2014, DOI 10.1074/jbc.M113.484162

Claudia Simon[‡], Thomas Klose[§], Sabine Herbst[¶], Bong Gyoon Han[‖], Andrea Sinz[¶], Robert M. Glaeser[‖], Milton T. Stubbs[‡], and Hauke Lilie[‡1]

From the [‡]Institute of Biochemistry and Biotechnology, Martin-Luther-University Halle-Wittenberg, Kurt-Mothes Strasse 03, 06120 Halle, Germany, the [§]Department of Biological Sciences, Purdue University, West Lafayette, Indiana 47907, the [¶]Institute of Pharmacy, Martin-Luther-University Halle-Wittenberg, Wolfgang-Langenbeck Strasse 04, 06120 Halle, Germany, and the [‖]Life Sciences Division, Lawrence Berkeley National Laboratory, University of California, Berkeley, California 94720

Background: Polyoma virus-like particles produced *in vivo* (yVLPs) are more stable than those assembled *in vitro*.
Results: yVLPs exhibit higher disulfide connectivity and additional N-terminal structural features in VP1.
Conclusion: An ordered network of cystine-bridged VP1 N-terminal peptides contributes to polyoma virus capsid stability.
Significance: These results suggest a role for intracellular components in optimizing capsid assembly.

VP1 is the major coat protein of murine polyomavirus and forms virus-like particles (VLPs) *in vitro*. VLPs consist of 72 pentameric VP1 subunits held together by a terminal clamp structure that is further stabilized by disulfide bonds and chelation of calcium ions. Yeast-derived VLPs (yVLPs) assemble intracellularly *in vivo* during recombinant protein production. These *in vivo* assembled yVLPs differ in several properties from VLPs assembled *in vitro* from bacterially produced pentamers. We found several intermolecular disulfide linkages in yVLPs involving 5 of the 6 cysteines of VP1 (Cys^{115}–Cys^{20}, Cys^{12}–Cys^{20}, Cys^{16}–Cys^{16}, Cys^{12}/ Cys^{16}–Cys^{115}, and Cys^{274}–Cys^{274}), indicating a highly coordinated disulfide network within the *in vivo* assembled particles involving the N-terminal region of VP1. Cryoelectron microscopy revealed structured termini not resolved in the published crystal structure of the bacterially expressed VLP that appear to clamp the pentameric subunits together. These structural features are probably the reason for the observed higher stability of *in vivo* assembled yVLPs compared with *in vitro* assembled bacterially expressed VLPs as monitored by increased thermal stability, higher resistance to trypsin cleavage, and a higher activation enthalpy of the disassembly reaction. This high stability is decreased following disassembly of yVLPs and subsequent *in vitro* reassembly, suggesting a role for cellular components in optimal assembly.

Murine polyomavirus is a nonenveloped dsDNA virus with a circular double-stranded DNA that is condensed with cellular host histones. The capsid of the virus is constructed from the three structural proteins VP1, VP2 and VP3, of which VP1 is the major coat protein. The pentameric VP1 represents the assembly subunit of the exterior shell and associates with the minor coat protein VP2 or VP3, which forms the interior shell of the capsid. The exterior shell resembles an icosahedron containing 12 pentavalent subunits with a 5-fold rotational symmetry at the vertices and 60 hexavalent pentameric subunits at the edges and faces of the icosahedral structure. The N termini of each pentamer interact with the C termini of neighboring pentamers in the VLP,[2] forming a clamp-like structure, further stabilized by disulfide formation and chelation of calcium (1). The capsid subunits are produced in the cytosol and transported to the nucleus (2), where they assemble to the viral capsid and pack viral DNA in so-called "nuclear virus factories" (3). Less is known about the ensuing maturation processes *in vivo* that follow until release from the cell. In particular, it is unclear at what point of viral assembly/maturation disulfide bonding takes place. VP1 contains six cysteines, and analysis of the viral uncoating process in the endoplasmic reticulum has revealed the existence of disulfides that are shuffled during capsid processing and are necessary for infection (4), yet only one disulfide bridge could be identified in the crystal structure (1). The viral capsid must be able to achieve multiple functions; it must protect the viral DNA against extracellular environmental stresses such as radiation, dryness, salt, and DNases but also facilitate receptor-mediated endocytosis (5), cellular trafficking (6, 7), uncoating (4), and finally gene release in the nucleus.

Following recombinant expression in bacteria (8, 9), VP1 is obtained in its pentameric form. These pentameric subunits alone can be assembled into virus-like particles *in vitro* (10) that resemble icosahedra. VLPs can be disassembled into their pentameric subunits (10) simply by adding reducing *and* chelating agents in the absence of stabilizing salts.

VP1 has also been expressed in eukaryotic systems, including insect cells (11) and yeast (12, 13). In these cases, VP1 is found only in an icosahedral VLP form. It has been shown that VLPs expressed in yeast harbor cellular nucleic acids (12) and are more stable than bacterial VP1 VLPs with regard to disassembly and limited proteolysis (14). Here, we present biophysical and structural data characterizing the VLPs produced in yeast and

* This work was supported by Deutsche Forschungsgemeinschaft Grant GRK 1026.
[S] This article contains supplemental 1.
[1] To whom correspondence should be addressed. E-mail: hauke.lilie@biochemtech.uni-halle.de.

[2] The abbreviations used are: VLP, virus-like particle; bVLPs, *in vitro* assembled VLPs from bacteria produced VP1 subunits; yVLP, *in vivo* assembled VLPs produced in yeast *Kluyveromyces lactis*; TCEP, tris(2-carboxyethyl)phosphine.

assembled *in vivo* ("yVLPs"), identify disulfide cross-links, and compare these results with those of conventionally *in vitro* assembled VLPs from VP1 produced in bacteria ("bVLPs").

EXPERIMENTAL PROCEDURES

Purification of yVLPs from Kluyveromyces lactis—VP1 (small plaque strain 16) was recombinantly expressed in the yeast strain *K. lactis* KD1/VP1 by high cell density fermentation, and intracellularly assembled VLPs were purified chromatographically as described previously (14). Briefly, VLPs were enriched from cell lysate by ammonium sulfate precipitation, followed by size exclusion (Superdex S200, GE Healthcare) and cation exchange chromatography (HiTrap HP SP, GE Healthcare) and a final size exclusion run (Superdex S500, GE Healthcare).

In Vitro Assembled bVLPs from Bacterial VP1—VP1 was recombinantly expressed in *Escherichia coli,* and pentameric VP1 was purified as described (8). Purified VP1 pentamers were assembled into VLPs by dialysis for 24 h at 25 °C against 0.4 M ammonium sulfate, 200 mM NaCl, 5% (v/v) glycerol, 0.5 mM GSH, 4.5 mM GSSG, 2 mM $CaCl_2$, 50 mM Tris, pH 7.4. Assembled VLPs were separated from non-VLPs by size exclusion chromatography (Superdex S200, GE Healthcare).

Temperature Transitions of VLPs—Temperature-induced denaturation of VLPs was monitored by fluorescence spectroscopy (excitation 280 nm, emission 340 nm). 600 nM VLPs in PBS (Jena Bioscience) were heated from 20 to 90 °C at a heating rate of 1 K min^{-1} using a Fluoromax-3 (Horibo Jobin Yvon) equipped with a Peltier element (Wavelength Electronics, lfi-3751). Equilibration time was set to 1 min. Pentameric samples were generated by disassembly of VLPs with 20 mM TCEP and 10 mM EDTA at 20 °C for 2 h and measured immediately.

Analytical Ultracentrifugation—To discriminate between VLPs, higher oligomers and pentameric subunits samples were centrifuged at 20 °C, 40,000 rpm for pentamers, 10,000 rpm for VLPs in an An50Ti rotor. Scans were taken every 10 min.

Disassembly of VLPs—VLPs (0.1 mg/ml in 50 mM Tris, pH 7.4, 200 mM NaCl, 5% (v/v) glycerol) were disassembled by adding 200 mM DTT and 50 mM EDTA at different temperatures (4–40 °C). The disassembly reaction was monitored by a decrease in the light scattering signal at 400 nm using a Fluoromax-4 (Horibo Jobin Yvon). As the disassembly of yVLPs was carried out in the presence of an excess of DTT, disulfide reduction is not a rate-limiting step, so the kinetics should reflect structural rearrangements. The rate constant k of every reaction was determined by a monoexponential (bVLPs) or biphasic exponential (yVLPs) fit. Activation enthalpies and activation entropies were determined from an Eyring plot.

To analyze disassembly products directly by analytical ultracentrifugation or fluorescence spectroscopy, we also disassembled VLPs with 20 mM TCEP, 10 mM EDTA in 0.3 M Tris, pH 7.4, 5% (v/v) glycerol, 200 mM NaCl 2 h at 20 °C. Note that using TCEP instead of DTT causes reduction of disulfides to become a rate-limiting step at the beginning of reaction and is therefore not suitable for kinetic studies.

Limited Proteolysis with Trypsin—VLPs (0.1 mg/ml) were treated with trypsin (Sigma) at a ratio of 5:1 (w/w) in 50 mM Tris, pH 7.4, 5% (v/v) glycerol, 200 mM NaCl, 20 mM DTT, and/or 10 mM EDTA. As trypsin activity is influenced by reducing and chelating agents, the disassembly conditions were modified accordingly. Samples were taken at several time points and immediately placed on ice, precipitated with 0.1% (w/v) sodium deoxycholate, 10% (w/v) TCA and analyzed with reducing SDS-PAGE. Bands corresponding to degradation products of VP1 were excised, digested *in gel* with chymotrypsin, and analyzed using nano-HPLC/nano-ESI-LTQ-Orbitrap-MS/MS (see below). Peptides were identified with the Proteome Discoverer 1.3 (ThermoFisher Scientific) using Mascot Server version 2.2. MS/MS experiments were reproduced at least twice. The disassembly process due to proteolysis was also monitored by measuring a decrease in the light scattering signal at 400 nm.

Reassembly of VLPs—1 mg/ml yeast VLPs were first disassembled in 300 mM Tris, pH 7.4, 200 mM NaCl, 5% (v/v) glycerol, 10 μg/ml RNase A (Peqlab) in the absence or presence of 10 mM EDTA and/or 20 mM TCEP for 2 h at 20 °C. Then the subunits were dialyzed against assembly buffer (0.8 M ammonium sulfate, 200 mM NaCl, 5% (v/v) glycerol, 0.5 mM GSH, 4.5 mM GSSG, 2 mM $CaCl_2$, 50 mM Tris, pH 6.4) to allow reassembly. After 48 h, the buffer was changed to the standard buffer 50 mM Tris, pH 7.4, 200 mM NaCl, 5% (v/v) glycerol by dialysis overnight. Although these conditions (low/neutral pH, high GSSG concentration) differ from those typically used for refolding processes, they are necessary to obtain reasonable VLP yields, as the assembly of VLPs is a highly cooperative process that is sensitive to pH and salt concentration (15). The disassembly and reassembly products were analyzed by analytical ultracentrifugation, transmission electron microscopy, temperature transitions, and disassembly studies.

Disulfide Pattern of Yeast VLPs—Intermolecular disulfide cross-links between VP1 monomers within the VLP were analyzed by LC/MS/MS on an Ultimate 3000 nano-HPLC system that was coupled on line to an LTQ-Orbitrap XL mass spectrometer (ThermoFisher Scientific) equipped with a nano-electrospray ionization source (Proxeon). 7 μg of VLPs in PBS, pH 6.0, were denatured with 8 M urea, optionally reduced with 10 mM DTT, alkylated with 55 mM iodoacetamide, and digested in solution with pepsin and 1% (w/v) TCA. Data were analyzed using the Proteome Discoverer 1.3, Xcalibur 2.07 (ThermoFisher Scientific) and StavroX 2.05 (16). MS/MS experiments were reproduced at least twice.

Cryo-EM and Data Analysis—Purified VLPs (1 mg/ml in 50 mM Tris, 200 mM NaCl, 5% (v/v) glycerol, pH 7.4) were placed on a glow discharged holey carbon copper grid (Quantifoil). The grid was loaded into a Vitrobot (FEI) at room temperature and 80–100% humidity, blotted for 3 s with filter paper, and plunged into liquid ethane for cryoelectron microscopy. The cryo-EM images were recorded on Kodak SO-163 film at a magnification of ×38,000 using a Philipps CM 200 transmission electron microscope at 200 kV with defocus values of 1–1.5 μm. Low dose conditions with an exposure of ~20 electrons/$Å^2$ per image were used. Images were digitized using the Nikon Super Coolscan 8000 ED densitometer (17). The images were scanned with a resolution of 6.35 μm per pixel and later averaged 2-fold in each direction, resulting in a resolution of 3.34 Å/pixel at the sample level. 2523 particles were boxed with the program EMAN Boxer (18) and used for the refinement. The defocus value of each micrograph was estimated by ctffind3, and phase

flipping was applied for each particle by using the SPIDER software package (19). A geometrical shell was used as a starting model. The orientations and translational alignments of the particle images were refined iteratively against the model by projection matching in SPIDER. Icosahedral symmetry was imposed during the refinement. The progress of the iterative refinement was initially monitored by the improvement of the Fourier shell correlation curve, which changed little after around 12 cycles. Docking of the atomic model into EM densities and display were carried out using UCSF Chimera (20) or PyMOL (21) as a further validation. The resolution of the three-dimensional reconstitution was estimated based on the Fourier shell correlation curve, which cuts off to 0.5 at 20 Å.

RESULTS

Disulfides of VLPs—VP1 contains six cysteines (Fig. 1). Published x-ray structures of viral particles (Protein Data Bank code 1SID (1)) show intermolecular, intrapentameric disulfide bonds between cysteine 115 and cysteine 20 in all but the pentavalent "5-fold axis" pentamers. No other disulfide bonds were observed in the crystal structure, although the presence of additional disulfide bonds in the VLPs has been described (4) (also for homologous polyomavirus SV40 (22–24)), but cross-links have not been assigned. Cysteine connectivities within the VLPs were therefore analyzed using pepsin cleavage in combination with tandem mass spectrometry (see supplement 1 for representative MS/MS spectra). Comparison of the sequence coverage analysis of reduced and nonreduced VLPs (Table 1) allowed quantification of disulfide cross-links. We found that Cys^{115} is quantitatively linked with one of the N-terminal cysteines Cys^{12}, Cys^{16}, or Cys^{20} (within the presumed flexible N-terminal region of VP1) in both yVLPs and bVLPs. All VLPs also showed a nonquantitative disulfide bond between Cys^{274} and Cys^{274}. Conversely, yVLPs possessed additional disulfide bonds between Cys^{16} and Cys^{16} and Cys^{12} and Cys^{20} that were not found in bVLPs, suggesting that VP1 subunits are highly connected by disulfides in yVLPs.

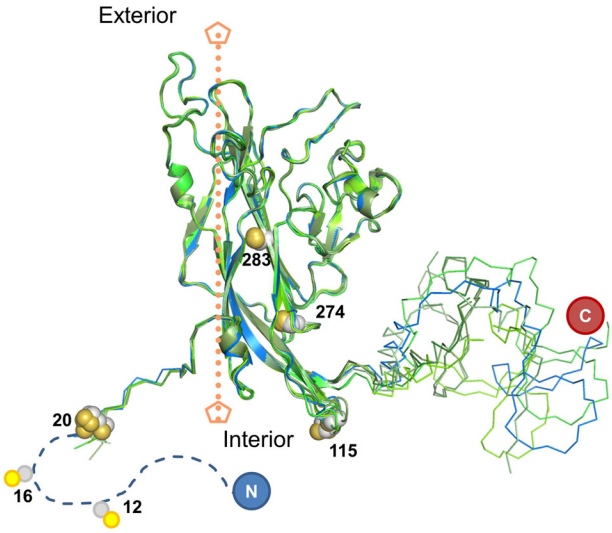

FIGURE 1. **Schematic view showing positions of cysteines in VP1.** VP1 has six cysteines (*spheres*), three of which are located in the N-terminal region and three in the core domain; the position of the 5-fold axis relating monomers in each pentamer is shown. In the assembled capsid, the region between Cys^{20} and the core domain forms a clamp-like structure with the C-terminal residues of a neighboring monomer, which adopt different conformations depending on their position in the capsid (pentavalent (*blue*) and hexavalent (*shades of green*) pentamers).

Thermal Stability of VLPs—Temperature-induced denaturation of VLPs revealed a significant difference in thermal stability for yVLPs compared with bVLPs and *in vitro* reassembled yVLPs. Whereas the thermal transition of bVLPs is characterized by a temperature midpoint of denaturation of $T_M = 50$ °C under the given conditions, yVLPs showed a T_M of 56 °C (Fig. 2). These values correspond to the stability of the VLPs and not just to that of the structured protein VP1, as pentameric VP1 generated by disassembly of either yVLPs or bVLPs exhibited a T_M of 46 °C (Fig. 2*A*). *In vitro* reassembly of pentameric VP1 from yVLPs resulted in VLPs with a temperature midpoint of denaturation ($T_M = 50$ °C) lower than the original yVLPs and similar to that of bVLPs, demonstrating a fundamental difference between *in vitro* reassembled VLPs and *in vivo* assembled yVLPs.

To analyze the influence of disulfide bonds on thermal stability, we reduced yVLPs with TCEP, which led to complete reduction of all disulfide bonds as determined by nonreducing SDS-PAGE (data not shown). Reduced yVLPs showed only a slightly lower thermal stability ($T_M = 53$ °C) compared with original yVLPs, but still a much higher thermal stability compared with bVLPs (Fig. 2) and reassembled VLPs. Reoxidation of reduced yVLPs resulted in thermal stabilities comparable with original yVLPs, and tandem mass spectrometry once again revealed the yVLP-specific disulfide pattern in reoxidized yVLPs not found in bVLPs (Table 1). These data suggest that additional structural elements stabilize *in vivo* assembled

TABLE 1

Disulfide cross-links of VLPs analyzed by MS/MS spectrometry

VLPs were cleaved with pepsin under reducing and nonreducing conditions (where cystines are maintained) and analyzed by tandem mass spectrometry. Sequence coverage was analyzed according to found peptides of VP1, and additionally data were screened for disulfide cross-links. Location of cysteines within a VP1 molecule is shown in Fig. 1. MS/MS spectra of cross-links can be found in the supplemental material.

	***In vitro* assembled bVLPs**	***In vivo* assembled yVLPs**
Sequence coverage of reduced samples (% of 384 amino acids)	97	98
Sequence coverage of nonreduced samples (% of 384 amino acids) including/excluding disulfide cross-links	93/84	93/84
Disulfide cross-links (present under nonreducing conditions only)	Cys^{115}–Cys^{12} or Cys^{16} or Cys^{20} *e.g.* (Asp^{112}–Thr^{117}) to (Lys^{11}–Leu^{30}) Cys^{274}–Cys^{274} *e.g.* (Leu^{265}–Leu^{279}) to (Leu^{265}–Gly^{279})	Cys^{115}–Cys^{12} or Cys^{16} or Cys^{20} *e.g.* (Asp^{112}–Thr^{117}) to (Lys^{11}–Leu^{30}) Cys^{274}–Cys^{274} *e.g.* (Leu^{265}–Leu^{279}) to (Leu^{265}–Gly^{279}) Cys12–Cys^{20} *e.g.* (Gly^{8}–Glu^{13}) to (Cys^{20}–Leu^{38}) Cys^{16}–Cys^{16} *e.g.* (Lys^{15}–Leu^{40}) to (Met^{1}–Thr^{17})

yVLPs compared with *in vitro* assembled VLPs and are maintained in yVLPs even after disulfide reduction, guiding correct disulfide bond formation upon reoxidation.

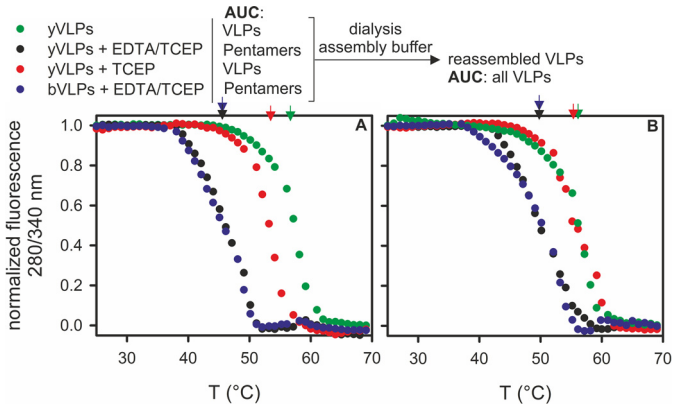

FIGURE 2. **Temperature-induced denaturation of VP1 pentamers and VLPs.** 600 nM of differently treated VLPs or VP1 pentamers were incubated in PBS at a heating rate of 1 K min^{-1}, and the protein fluorescence ($\lambda_{exc.}$ = 280 nm, $\lambda_{em.}$ = 340 nm) was monitored. *A,* yVLPs were treated with 20 mM TCEP (*red*), 20 mM TCEP, and 10 mM EDTA (*black*), or without TCEP/EDTA (*green*). As a control, bVLPs (*blue*) were incubated with 20 mM TCEP and 10 mM EDTA for 2 h at 20 °C. Analytical ultracentrifugation (*AUC*) showed that only the samples treated with TCEP and EDTA disassembled completely into pentameric subunits. *B,* all samples were dialyzed 48 h at 25 °C against assembly buffer to allow reassembly and/or reoxidation. Reassembly to homogeneous VLPs was again verified by analytical ultracentrifugation. T_M values of each transition are indicated by *arrows above* the graphs. Pentameric subunits of both yVLPs and bVLPs (T_M = 46 °C) as well as their reassembled VLPs (T_M = 50 °C) show a lower thermal stability compared with untreated yVLPs (T_M = 56 °C). The thermal stability of reduced VLPs was only slightly decreased (T_M = 53 °C), and the reoxidized VLPs show a thermal stability similar to original yVLPs.

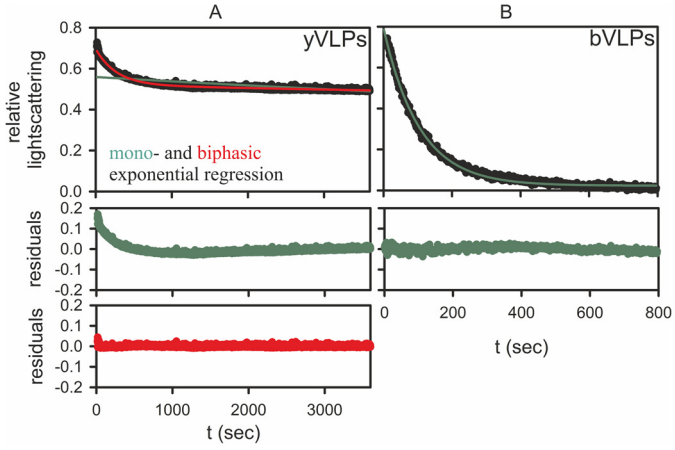

FIGURE 3. **Disassembly kinetics of yVLPs.** *A,* yVLPs were disassembled with 200 mM DTT and 50 mM EDTA at pH 7.4 and 25 °C, and the reaction was monitored by light scattering. Data were fitted by monophasic (*green*) and biphasic (*red*) exponential regression. The residuals for both fits clearly demonstrate a biphasic disassembly of yeast VLPs. The biphasic fit extrapolates to a final signal of relative light scattering of 0.25 after 12 h. *B,* disassembly kinetics of bVLPs measured under identical conditions exhibit a single first-order reaction (*green line*).

Disassembly of VLPs—Another possibility to gain insight into the stability of VLPs is to monitor the kinetics of the disassembly into their subunits, whereby the temperature dependence provides information about enthalpic and entropic contributions to this reaction.

The disassembly reaction was started by addition of DTT and EDTA and monitored by light scattering. The disassembly kinetics of bVLPs could be fitted to a comparably fast and monophasic reaction (k = 0.015 s^{-1} at 25 °C, Fig. 3*B*), whereas the disassembly reaction of yVLPs was much slower and exhibited at least two phases (Fig. 3*A*). As it is known that *in vivo* assembled VLPs contain nucleic acids (12, 25), here RNA, the disassembly was also monitored in the presence of a nuclease. Addition of an excess of RNase A to the disassembly reaction still resulted in a biphasic reaction, with rate constants similar to the reaction in the absence of RNase, but the amplitude of the slow phase decreased significantly (Table 2), and the amplitude of the fast reaction increased in a compensatory fashion. Further analyses of the purified yVLPs indicated that the majority of particles contained nucleic acids of a size between 100 and 500 bases (average 300 bases) that could be digested completely by RNase A but not by DNase I, indicating incorporation of RNA into the yVLPs (data not shown). We therefore conclude that the slower yVLP disassembly reaction (k_2 = 0.0002 s^{-1} at 25 °C) is dominated by RNA-VLP interactions and thus does not describe a specific molecular process upon disassembly. However, the fast yVLP disassembly reaction corresponds to the disassembly of nucleic acid-free VLPs (k_1 = 0.0028 s^{-1} at 25 °C), which is still about 2 orders of magnitude slower than that of bVLPs or *in vitro* reassembled yVLPs.

In addition, the temperature dependence of the rate of disassembly reaction 1 (k_1, Fig. 4) indicated a very high activation enthalpy of ΔH^* = 103 kJ mol^{-1} but a favorable activation entropy. This is quite different for the disassembly of bVLPs, which exhibited a strongly unfavorable activation entropy (Fig. 4 and Table 3). These differences in activation enthalpy ΔH^* and activation entropy ΔS^* indicate that the energy barrier of the disassembly reaction is governed at least in part by different molecular interactions in yVLPs and bVLPs.

To find out if the observed disulfide bond Cys^{274}–Cys^{274} contributes significantly to the stability of the VLPs, we compared wild type yVLPs with a cysteine variant C274S yVLPs and could detect no significant differences in thermal stability or disassembly kinetics (Table 3 and Fig. 5).

Trypsin-induced Disassembly of VLPs—Commonly, disassembly of polyoma VLPs can be induced chemically by addition of chelating and reducing agents, such as EDTA and DTT. As described previously, bVLPs can also be disassembled into pentameric VP1 by addition of trypsin (14). In contrast, yVLPs proved resistant to trypsin both in the absence (14) and pres-

TABLE 2

Effect of RNase A (10 μg/ml) on disassembly of 0.1 mg/ml yeast VLPs with 200 mM DTT and 50 mM EDTA at pH 7.4 and 25 °C

The reaction was monitored by light scattering, and data were fitted with a biphasic exponential regression. The rate constants k_1 and k_2 refer to the fast and slow phases of disassembly, respectively.

RNase A	k_1 (s^{-1})·10^{-3}	k_2 (s^{-1})·10^{-3}	Relative amplitude phase 1	Relative amplitude phase 2
With	1.9 ± 0.057	0.3 ± 0.009	0.51	0.49
Without	2.8 ± 0.162	0.2 ± 0.012	0.30	0.70

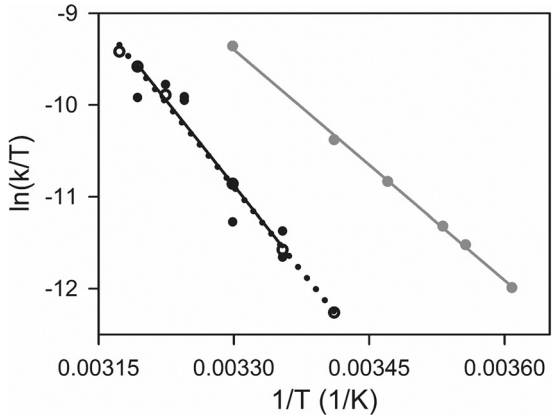

FIGURE 4. **Eyring plot of disassembly reactions of VLPs.** VLPs were disassembled by addition of 200 mM DTT and 50 mM EDTA at different temperatures, and the reaction was monitored by light scattering. Rate constants were determined by mono- (bVLPs) or biexponential (yVLPs) fits, and k (bVLPs) and k_1 ("RNA-independent" rate of yVLPs) were plotted according to Eyring. All fitted parameters are listed in Table 3. *Black symbol* and *black line,* WT yVLPs; *open circle* and *dotted line,* C274S yVLPs; *gray symbols* and *gray line,* bVLPs.

TABLE 3

Kinetic stability of VLPs

For A, "RNA-independent" rate constants of disassembly (k_1) of 0.1 mg/ml VLPs were induced with 200 mM DTT and 50 mM EDTA at pH 7.4 and 25 °C and monitored by light scattering. Data were fitted with a monophasic (bVLPs) or biphasic (yVLPs) exponential regression. For B, mid-points of temperature-induced denaturation of VLPs at pH 7.4 were monitored by fluorescence ($\lambda_{exc.}$ 280 nm and $\lambda_{em.}$ 340 nm). For C, thermodynamic parameters of the disassembly reaction were calculated from the temperature-dependent disassembly of VLPs analyzed according to Eyring (Fig. 4).

	VLPs, VP1	yVLPs WT	yVLPs tC274S	bVLPs WT
A	$k{\cdot}10^{-3}$ (s^{-1}) at 25 °C, pH 7.4	3 ± 0.171 (k_1)	3 ± 0.177 (k_1)	15 ± 0.03
B	T_M (°C), pH 7.4	56 ± 0.1	56 ± 0.2	50 ± 0.2
C	ΔH^* (kJ mol^{-1})	103 ± 1.2	101 ± 0.1	70 ± 0.07
	ΔS^* (J mol^{-1} K^{-1})	51 ± 0.6	47 ± 0.05	−46 ± 0.05
	ΔG^* 37 °C (kJ mol^{-1})	87 ± 1.04	87 ± 0.09	84 ± 0.08

ence of EDTA (data not shown) but not in presence of DTT alone (Fig. 5). Trypsin accelerated the disassembly of yVLPs in the presence of DTT and EDTA (Fig. 5), however. Following this disassembly process by reducing SDS-PAGE revealed a time-dependent degradation of full-length VP1 to a stable product of about 35 kDa (Fig. 5*B*, *species 4*) via two dominant intermediates. The time course of the occurrence of this proteolytic end product parallels complete disassembly. We excised the four distinct bands, performed an *in gel* digestion with chymotrypsin, and analyzed the peptide mixture by nano-HPLC/nano-ESI-LTQ-Orbitrap-MS. Species 1 (Fig. 5*B*) showed 99.74% sequence coverage of VP1, missing only the start methionine, so that any missing peptides in the remaining species can be attributed to trypsin proteolysis and not to the experimental procedure. The respective cleavage sites of the different species are shown in Fig. 5*C*; only species 4 corresponds to completely disassembled VLPs. Proteolysis in species 4 takes place in the N-terminal clamp structure of VP1 that fixes the C-terminal arm of the neighboring pentamers (Fig. 5*C*). Whereas these cleavage sites are accessible to trypsin in bVLPs, they are only cleaved in yVLPs in the presence of at least DTT, suggesting that the N-terminal peptides in yVLPs possess an ordered structure that is protected by disulfide bond formation.

Structural Analysis by Cryo-EM Image Reconstruction—We used cryoelectron microscopy to obtain more information on the structure of the yVLPs. Single particle cryo-EM reconstructions show the expected icosahedral arrangement of the 72 pentameric subunits with typical 5- and 3-fold symmetries at a nominal resolution of 20 Å. The density corresponds well to the x-ray structure of *in vitro* reconstituted bVLPs (Fig. 6*A*, Protein Data Bank code 1SID (1)), but reveals additional foot-shaped structural features in the interior of the particles (Fig. 6*B*). Each foot (whose volume is consistent with ~100 amino acid residues) originates at the converging positions of the N-terminal Cys^{20} residues of three adjacent pentamers surrounding the 5-fold axis ("pentavalent pentamers," Fig. 6*B*), and proceeds toward the N-terminal Cys^{20} residues of two adjacent pentamers surrounding the 3-fold axis (Fig. 6*C*). The reconstruction therefore suggests that the cysteine-rich N termini form a globular domain by inter-digitating to link adjacent 5-fold symmetric hexamers of pentamers.

DISCUSSION

Previous crystal structures of icosahedral polyoma VP1 virus-like particles (1), which consist of 12 pentavalent and 60 hexavalent pentameric subunits, have demonstrated that the capsids are stabilized in three ways as follows: through formation of a clamp-like structure from the N- and C-terminal peptides of individual pentamers, through Ca^{2+} binding, and through intermonomeric/intrapentameric disulfide bond formation between Cys^{20} and Cys^{115} (in hexavalent pentamers only). Despite the similarity in morphology of *in vitro* assembled bVLPs and yeast-derived yVLPs, there exist marked differences between the two preparations. Compared with bVLPs, yVLPs are more stable and rigid and disassemble at a slower rate, with a higher activation enthalpy and entropy. MS/MS data of yVLPs revealed the presence of disulfides (Cys^{12}–Cys^{20} and Cys^{16}–Cys^{16}) that presumably link the N termini of VP1 of different pentamers. Such disulfides were not observable in the previous crystal structure, which shows no electron density for the first 17 amino acids (1). Our data on bVLPs suggest the absence of these disulfides in *in vitro* assembled material. We further found evidence for the presence of disulfide bridges between Cys^{115} and either Cys^{12} or Cys^{16} in both bVLPs and yVLPs, as well as a nonquantitative Cys^{274}–Cys^{274} linkage. The cryo-EM reconstruction clearly shows additional highly ordered electron densities at the N-terminal regions of VP1 in the VLPs, with sufficient volume to encompass three to four VP1 N termini from neighboring pentamers, providing space for the formation of the above described intrapentameric disulfide bridges. Within the pentavalent pentamers, the highly conserved Cys^{115} (which is not cross-linked with Cys^{20} here) lies in close proximity to the N-terminal cysteines Cys^{12} and Cys^{16} of adjacent monomers, providing an explanation for the observed Cys^{115}–Cys^{12}/Cys^{16} disulfide. Because the distance between the "pentavalent" Cys^{20}/Cys^{115} thiol groups and those surrounding the 3-fold axes are ~40 Å in the crystal structure, the observed disulfide bridges (and densities) cannot simply be a covalent linkage connecting neighboring pentavalent and

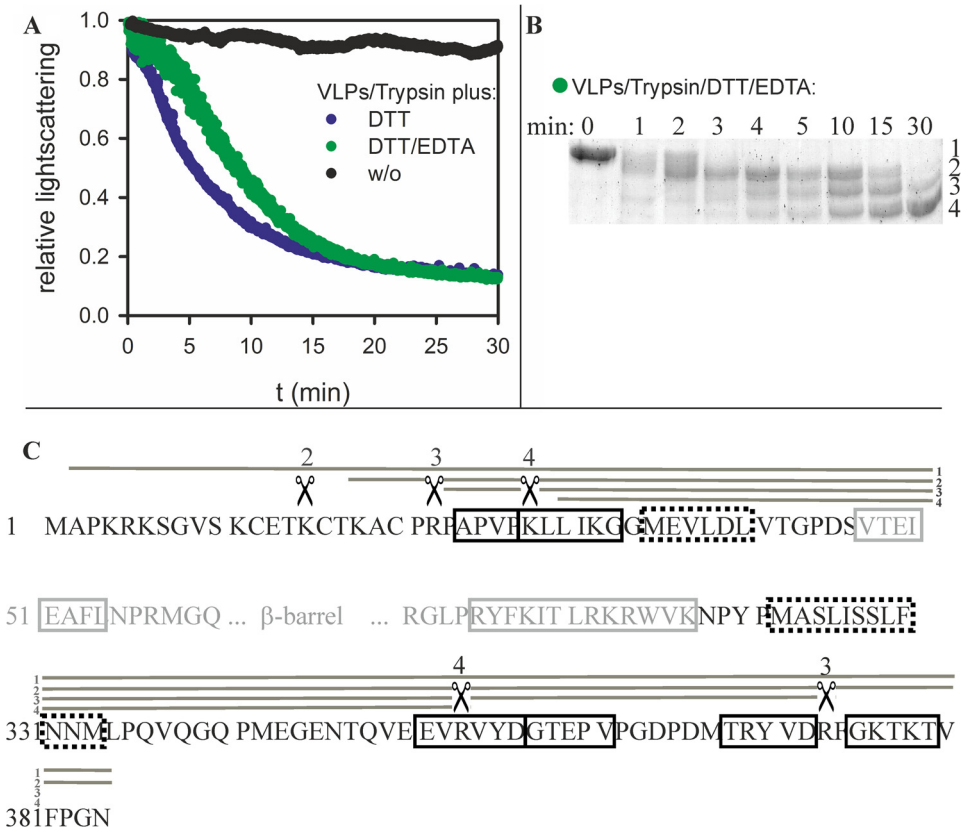

FIGURE 5. **Disassembly of yVLPs with trypsin.** *A,* yVLPs were treated with trypsin (*black*), trypsin, 20 mM DTT, 10 mM EDTA (*green*), or trypsin/20 mM DTT (*blue*), respectively, at pH 7. 4 and 37 °C. *B,* samples of the disassembly reaction in the presence of trypsin, 20 mM DTT, 10 mM EDTA were taken at the indicated time points and analyzed by reducing SDS-PAGE. *C,* four gel bands corresponding to degradation products of VP1 were excised and analyzed by LC/MS/MS. The schematic view shows only the N and C termini of VP1 (*black*), omitting the β-barrel domain (*gray*). *Solid lined boxes* depict β-sheets, and *boxes* with *dashed lines* depict α-helices of the assembled VLP (modified after Ref. 30). The *gray lines above* the sequence of the termini demonstrate the sequence coverage of the respective degradation product (*species 1–4*), and the *numbered scissors* indicate the trypsin cleavage sites for each species. Cleavage sites of band 4 are located in the clamp structure of the VLP. Cleavage at position 4 mediates disassembly of VLPs.

hexavalent pentamers. Instead, we suppose that the N-terminal peptides intertwine to form defined globular domains with intermonomeric disulfide linkages.

Disulfide bonds are known to increase the thermal stability of viral capsids (26, 27). In this study, reduction of disulfide bonds only slightly decreased thermal stability of yVLPs compared with the original yVLPs. The additional interpentameric contacts represented by the foot-like structures are likely to be responsible for the higher stability in yVLPs, with the observed yVLP-specific disulfides providing additional rigidity to these structures, as disulfide reduction is required for trypsin-mediated yVLP disassembly; bVLPs, however (which exhibit no cross-links between N-terminal cysteines), are not protected against proteolysis in the absence of any reducing agent. However, disulfide bonds in bVLPs (and yVLPs) protect the VLPs against chemically induced disassembly under chelating conditions.

Alternatively, the cross-links may represent deviations from icosahedral symmetry within the VLPs. Although we deem this to be unlikely, the presence of the Cys^{274}–Cys^{274} disulfide cannot be explained by either the published crystal structures or the EM structure presented here. This bond does not seem to affect the stability of VLPs, as we found no differences in thermal stability, disassembly, or disassembly activation barrier for the C274S variant VP1 yVLPs. Conversely, Cys^{274} is (along with Cys^{115}) the most conserved cysteine in VP1 of all polyomaviruses, and mutations lead to a tremendous decrease in virus infectivity as has been shown previously for the related polyomavirus SV40 (28). The presence of this bond in substoichiometric quantities may therefore be an indication of significant local deviations from strict icosahedral symmetry.

The higher stability of VLPs recombinantly expressed in eukaryotes was already reported qualitatively for expression in *Saccharomyces cerevisiae* and insect cells (13, 29). Because yVLPs exhibit a stronger association of pentameric subunits compared with bVLPs, we assume that intertwining of the N-terminal regions, complemented by N-terminal disulfide cross-links, supplements the previously described clamp structure (30). The existence of N-terminal disulfide linkages has long been thought to cross-link different VP1 pentamers (4), and similar interpentameric N-terminal cysteine linkages have been discussed for VP1 in polyomavirus SV40 (22–24). Although we are unable to distinguish between cystine formation occurring in the course of *in vivo* yVLP assembly or extracellularly/post-purification, *in vitro* assembly of VP1 into bVLPs under well defined redox conditions shows that disulfide bond formation takes place only after VLP assembly.[3] Furthermore, a VP1 variant in which all cysteines have

[3] T. Klose and H. Lilie, unpublished data.

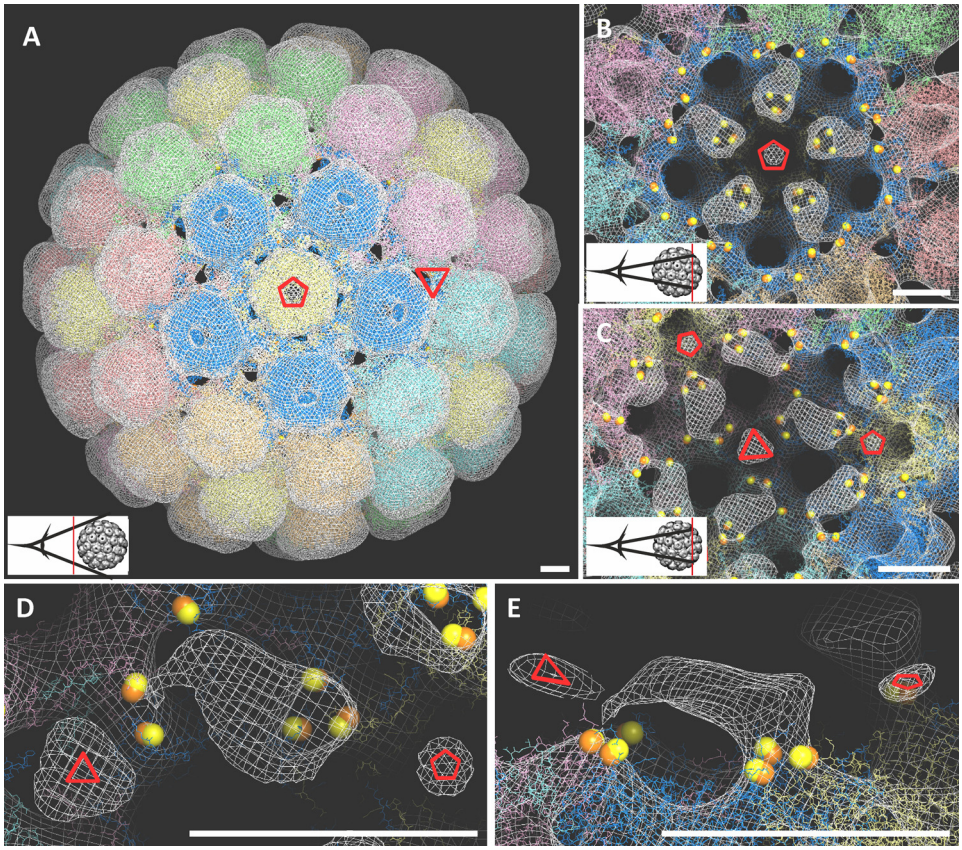

FIGURE 6. **Foot-shaped structures in the interior of yVLPs.** The cryo-EM reconstruction of yVLPs is superimposed with the crystal structure of bVLP (Protein Data Bank code 1SID (1)). Each hexamer of pentamers (consisting of one pentavalent pentamer in *yellow*) and five adjacent "hexavalent" pentamers (*blue* in the foremost asymmetric unit) are colored differently for orientation purposes. The overlaid *red pentagon* and *triangles* depict the icosahedral 5- and 3-fold axes, respectively. *A,* view from the outside of the particle down the 5-fold axis demonstrates the excellent overall agreement between the cryo-EM reconstruction and the bVLP crystal structure. *B,* viewing the interior of the particle by rotating 180° about a vertical axis from *A* reveals additional foot-shaped densities that connect pentamers around the 5-fold axis with pentamers surrounding the 3-fold axes (*C*). The *spheres*, corresponding to individual sulfur atoms of cysteine 115 (*orange*) and cysteine 20 (*yellow*), serve to mark the positions of the N termini (prior to cysteine 20) not present in the bVLP structure (1). *D* and *E,* magnification of the density feature, oriented *D* as in *C* or rotated 90° about a horizontal axis. *E* shows that the density originates at the confluence of three N termini surrounding the pentavalent VP1 pentamer (the "ankle") and progresses toward at least one N terminus near the 3-fold axis (the "toe"). The volume of the foot density (ankle, heel, and toe) is consistent with a total of ~100 amino acid residues. The *white bars* in the panels represent 50 Å.

been substituted by serine is still able to form VLPs (31), clearly indicating that disulfides are not essential for the assembly process. However, it is conceivable that the very high local concentration of cysteines resulting from ordering of the N-terminal VP1 structure in the *in vivo* assembled yVLPs could induce disulfide formation, even under intracellular reducing conditions. We observed that *in vitro* reassembly of disassembled yVLPs results in particles of lower stability, similar to that of bVLPs, suggesting a role for host cell factors during intracellular assembly in yeast. Such cellular "assembly helpers" might include the following: (i) interaction of VP1 with cellular RNA and assembly of VLPs in the yeast nuclei (12), as the natural virus assembles in so-called "nuclear cell factories" (3); (ii) cellular chaperones or protein isomerases, which are known to interact with VP1 *in vivo* (32) and can induce assembly of VP1 into VLPs *in vitro* (33); and (iii) cytoskeletal and nuclear matrix proteins, which have been shown to interact with VP1 during expression (12, 34). Even though the assembly of VLPs *in vitro* is a spontaneous process (10) under appropriate conditions, cellular factors might control and direct this process to increase the efficacy of assembly and the structural homogeneity of viral capsids.

Acknowledgments—We thank Holger Herrmann for programming gradient simulations and data processing; Dr. Gerd Hause for negative staining EM; Dr. Roseann Csencsits for the cryo-EM microscope setup; Christian Arlt for support in MS/MS data collection; Marcus Boehme for support in disassembly data collection, and Robert L. Garcea for providing the VP1 gene.

REFERENCES

1. Stehle, T., and Harrison, S. C. (1996) Crystal structures of murine polyomavirus in complex with straight-chain and branched-chain sialyloligosaccharide receptor fragments. *Structure* **4,** 183–194
2. Bird, G., O'Donnell, M., Moroianu, J., and Garcea, R. L. (2008) Possible role for cellular karyopherins in regulating polyomavirus and papillomavirus capsid assembly. *J. Virol.* **82,** 9848–9857
3. Erickson, K. D., Bouchet-Marquis, C., Heiser, K., Szomolanyi-Tsuda, E., Mishra, R., Lamothe, B., Hoenger, A., and Garcea, R. L. (2012) Virion assembly factories in the nucleus of polyomavirus-infected cells. *PLoS Pathog.* **8,** e1002630
4. Walczak, C. P., and Tsai, B. (2011) A PDI family network acts distinctly and coordinately with ERp29 to facilitate polyomavirus infection. *J. Virol.*

85, 2386–2396
5. Richterová, Z., Liebl, D., Horák, M., Palková, Z., Stokrová, J., Hozák, P., Korb, J., and Forstová, J. (2001) Caveolae are involved in the trafficking of mouse polyomavirus virions and artificial VP1 pseudocapsids toward cell nuclei. *J. Virol.* **75,** 10880–10891
6. Inoue, T., and Tsai, B. (2011) A large and intact viral particle penetrates the endoplasmic reticulum membrane to reach the cytosol. *PLoS Pathog.* **7,** e1002037
7. Mannová, P., and Forstová, J. (2003) Mouse polyomavirus utilizes recycling endosomes for a traffic pathway independent of COPI vesicle transport. *J. Virol.* **77,** 1672–1681
8. Leavitt, A. D., Roberts, T. M., and Garcea, R. L. (1985) Polyoma virus major capsid protein, VP1. Purification after high level expression in *Escherichia coli*. *J. Biol. Chem.* **260,** 12803–12809
9. Liew, M. W., Rajendran, A., and Middelberg, A. P. (2010) Microbial production of virus-like particle vaccine protein at gram-per-litre levels. *J. Biotechnol.* **150,** 224–231
10. Salunke, D. M., Caspar, D. L., and Garcea, R. L. (1986) Self-assembly of purified polyomavirus capsid protein VP1. *Cell* **46,** 895–904
11. Montross, L., Watkins, S., Moreland, R. B., Mamon, H., Caspar, D. L., and Garcea, R. L. (1991) Nuclear assembly of polyomavirus capsids in insect cells expressing the major capsid protein VP1. *J. Virol.* **65,** 4991–4998
12. Palková, Z., Adamec, T., Liebl, D., Stokrová, J., and Forstová, J. (2000) Production of polyomavirus structural protein VP1 in yeast cells and its interaction with cell structures. *FEBS Lett.* **478,** 281–289
13. Sasnauskas, K., Buzaite, O., Vogel, F., Jandrig, B., Razanskas, R., Staniulis, J., Scherneck, S., Krüger, D. H., and Ulrich, R. (1999) Yeast cells allow high-level expression and formation of polyomavirus-like particles. *Biol. Chem.* **380,** 381–386
14. Simon, C., Schaepe, S., Breunig, K., and Lilie, H. (2013) Production of polyomavirus-like particles in a kLGAL80 knockout strain of the yeast *Kluyveromyces lactis*. *Prep. Biochem. Biotechnol.* **43,** 217–235
15. Salunke, D. M., Caspar, D. L., and Garcea, R. L. (1989) Polymorphism in the assembly of polyomavirus capsid protein VP1. *Biophys. J.* **56,** 887–900
16. Götze, M., Pettelkau, J., Schaks, S., Bosse, K., Ihling, C. H., Krauth, F., Fritzsche, R., Kühn, U., and Sinz, A. (2012) StavroX–A software for analyzing cross-linked products in protein interaction studies. *J. Am. Soc. Mass. Spectrom.* **23,** 76–87
17. Typke, D., Nordmeyer, R. A., Jones, A., Lee, J., Avila-Sakar, A., Downing, K. H., and Glaeser, R. M. (2005) High-throughput film-densitometry: An efficient approach to generate large data sets. *J. Struct. Biol.* **149,** 17–29
18. Ludtke, S. J., Baldwin, P. R., and Chiu, W. (1999) EMAN: Semiautomated software for high-resolution single-particle reconstructions. *J. Struct. Biol.* **128,** 82–97
19. Frank, J. (2006) *Three-dimensional Electron Microscopy of Macromolecular Assemblies–Visualization of Biology Cal Molecules in Their Native State*, 2 Ed., pp. 71–145, Oxford University Press, New York
20. Pettersen, E. F., Goddard, T. D., Huang, C. C., Couch, G. S., Greenblatt, D. M., Meng, E. C., and Ferrin, T. E. (2004) UCSF Chimera–A visualization system for exploratory research and analysis. *J. Comput. Chem.* **25,** 1605–1612
21. DeLano, W. L. (2002) *The PyMOL Molecular Graphics System.* DeLano Scientific LLC, San Carlos, CA
22. Jao, C. C., Weidman, M. K., Perez, A. R., and Gharakhanian, E. (1999) Cys9, Cys104 and Cys207 of simian virus 40 Vp1 are essential for interpentamer disulfide-linkage and stabilization in cell-free lysates. *J. Gen. Virol.* **80,** 2481–2489
23. Liddington, R. C., Yan, Y., Moulai, J., Sahli, R., Benjamin, T. L., and Harrison, S. C. (1991) Structure of simian virus 40 at 3.8-Å resolution. *Nature* **354,** 278–284
24. Schelhaas, M., Malmström, J., Pelkmans, L., Haugstetter, J., Ellgaard, L., Grünewald, K., and Helenius, A. (2007) Simian virus 40 depends on ER protein folding and quality control factors for entry into host cells. *Cell* **131,** 516–529
25. Sasnauskas, K., Bulavaite, A., Hale, A., Jin, L., Knowles, W. A., Gedvilaite, A., Dargeviciūte, A., Bartkeviciūte, D., Zvirbliene, A., Staniulis, J., Brown, D. W., and Ulrich, R. (2002) Generation of recombinant virus-like particles of human and non-human polyomaviruses in yeast *Saccharomyces cerevisiae*. *Intervirology* **45,** 308–317
26. Ashcroft, A. E., Lago, H., Macedo, J. M., Horn, W. T., Stonehouse, N. J., and Stockley, P. G. (2005) Engineering thermal stability in RNA phage capsids via disulphide bonds. *J. Nanosci. Nanotechnol.* **5,** 2034–2041
27. Bundy, B. C., and Swartz, J. R. (2011) Efficient disulfide bond formation in virus-like particles. *J. Biotechnol.* **154,** 230–239
28. Li, P. P., Nakanishi, A., Tran, M. A., Salazar, A. M., Liddington, R. C., and Kasamatsu, H. (2000) Role of simian virus 40 Vp1 cysteines in virion infectivity. *J. Virol.* **74,** 11388–11393
29. Chang, D., Fung, C. Y., Ou, W. C., Chao, P. C., Li, S. Y., Wang, M., Huang, Y. L., Tzeng, T. Y., and Tsai, R. T. (1997) Self-assembly of the JC virus major capsid protein, VP1, expressed in insect cells. *J. Gen. Virol.* **78,** 1435–1439
30. Stehle, T., and Harrison, S. C. (1997) High-resolution structure of a polyomavirus VP1-oligosaccharide complex: implications for assembly and receptor binding. *EMBO J.* **16,** 5139–5148
31. Schmidt, U., Rudolph, R., and Böhm, G. (2000) Mechanism of assembly of recombinant murine polyomavirus-like particles. *J. Virol.* **74,** 1658–1662
32. Cripe, T. P., Delos, S. E., Estes, P. A., and Garcea, R. L. (1995) *In vivo* and *in vitro* association of hsc70 with polyomavirus capsid proteins. *J. Virol.* **69,** 7807–7813
33. Chromy, L. R., Pipas, J. M., and Garcea, R. L. (2003) Chaperone-mediated *in vitro* assembly of polyomavirus capsids. *Proc. Natl. Acad. Sci. U.S.A.* **100,** 10477–10482
34. Palková, Z., Spanielová, H., Gottifredi, V., Hollanderová, D., Forstová, J., and Amati, P. (2000) The polyomavirus major capsid protein VP1 interacts with the nuclear matrix regulatory protein YY1. *FEBS Lett.* **467,** 359–364